International Journal of Adhesion and Adhesives 86 (2018) 45–58

Contents lists available at ScienceDirect

International Journal of Adhesion and Adhesives

journal homepage: www.elsevier.com/locate/ijadhadh

Most suitable evaluation method for adhesive strength to minimize bend effect in lap joints in terms of the intensity of singular stress field

Rong Li[a,c], Nao-Aki Noda[a,*], Rei Takaki[a], Yoshikazu Sano[a], Yasushi Takase[a], Tatsujiro Miyazaki[b]

[a] Department of Mechanical Engineering, Kyushu Institute of Technology, 1-1 Sensui-cho Tobata-ku, Kitakyushu-shi 804-8550, Japan
[b] Department of Mechanical Engineering, University of the Ryukyus, 1 Senbaru, Nishihara-cho, Nakagami-gun, Okinawa 903-0213, Japan
[c] School of Civil Engineering, Henan University of Science and Technology, Luoyang 471023, China

ARTICLE INFO

Keywords:
Adhesion
Fracture mechanics
Intensity of singular stress field
Interface
single lap joint

ABSTRACT

The lap joint testing is designed to investigate the adhesive strength under pure shear loading. However, actually pure shear testing is very difficult to be realized in the experiment because of the bend deformation during testing causing the peeling force appearing at the adhesive region. To reduce the bend effect, this paper focuses on the intensity of singular stress field (ISSF) at the interface end in order to minimize the ISSF for lap joints. The results show that the ISSF decreases with increasing the adherend thickness. The minimum ISSF is obtained when the adherend thickness is large enough with the small deformation angle defined at the interface end. Since the strength of double lap joint (DLJ) is sometimes about two times larger than the strength of single lap joint (SLJ), the equivalent strength condition is discussed by changing adherend thicknesses of DLJ and SLJ. It is found that the strength of SLJ with adherend thickness t_1 = 7 mm is nearly equal to that of double lap joint with t_1 = 1.5 mm prescribed in Japanese Industrial Standard.

1. Introduction

Due to the lower cost, high fatigue resistance and availability, structural adhesive has been widely used in a variety of industrial fields, such as automobile industry [1–4], shipbuilding [5,6], aircraft and spacecraft structures [7]. Structural adhesive has been replacing welding, screw, bolt, etc. It has been reported that the adhesive strength can be sometimes equivalent to the strength of the adherend [1,2]. Recently, the authors have shown that the adhesive strength is controlled by the intensity of the singular stress field (ISSF) at the interface end. As shown in Fig. 1(a) ~ (b), the butt joint strength can be expressed as a constant value of the critical ISSF $K_{\sigma c}$ = const. [8]. Also, as shown in Fig. 1(c) ~(d) the lap joint strength can be expressed as $K_{\sigma c}$ = const. [9–13]. Similarly, the adhesive bonded strength was previously expressed as H_{cr} = const in [14,15]. Since those previous studies indicated that the ISSF may control the adhesive strength [8–17], rational and practical ISSF methods can be used for evaluating the adhesive strength.

The testing method for the adhesive strength of lap joints is prescribed in Japanese Industrial Standards (JIS) [18]. However, usually the lap joint strength is affected by the specimen configuration. As an example, Fig. 2(a) shows that the critical average shear stress of the double lap joint (DLJ) strength is nearly twice larger than the one of the single lap joint (SLJ) strength [19,20]. Fig. 2(b) shows that the critical average shear stress leading to the results in Fig. 1(b) [21]. In Fig. 2(b), among the specimens A20-15 ~ A50-15 having different bondline length l_{ad}, the critical average shear stress τ_{ave} decreases with increasing the adhesive length. Therefore, Fig. 2(b) shows the adhesive strength cannot be expressed as τ_{ave} = const.

The SLJ testing was originally intended to be conducted under pure shear loading, but actually the pure shear testing is very difficult to be realized experimentally. Due to the bend deformation during testing, the peeling force is always generated to prevent pure shear testing at the adhesive region. Since this peeling force is corresponding to the ISSF at the interface end, this study focuses on how to minimize the ISSF for SLJ. Then, the effect of the specimen geometry on the ISSF will be discussed by considering the previous experimental studies [21]. Since the strength of DLJ is usually much larger than the strength of SLJ [19,20], the equivalent conditions for the single and double lap joints will be also discussed in this paper.

2. Lap joint modelling and mesh-independent technique to calculate the ISSF

In this section, the ISSF method to evaluate lap joint strength will be explained. The mesh-independent techniques to calculate the ISSF can

* Corresponding author.
E-mail address: noda@mech.kyutech.ac.jp (N.-A. Noda).

https://doi.org/10.1016/j.ijadhadh.2018.08.006
Accepted 9 August 2018
Available online 23 August 2018

Nomenclature

C_σ,C_τ	Constants defined as the ISSF ratio $C_\sigma = K_{\sigma,\lambda_2}/K_{\sigma,\lambda_1}$, $C_\tau = K_{\tau,\lambda_2}/K_{\tau,\lambda_1}$
e	Distance from center point of the loading surface to loading point
E	Young's modulus
G	Shear modulus
L	Fixed boundary length in Fig. 3(a), (b)
K_σ	ISSF, Intensity of singular stress field
$K_{\sigma c}$	Critical value of ISSF, critical intensity of singular stress field
l_1	Adherend length in Fig. 3(a), (b)
l_2	Adherend length $l_2 = l_1 - l_{ad} - d$ in Fig. 3(a), (b)
l_{ad}	Bondline length in Fig. 3(a), (b)
P	Load parameter $P/W = \sigma_o t = 14.15$ N/mm
r	Radial distance away from the corner point O in Fig. 3(a), (b)
t_1	Adherend thickness in Fig. 3(a), (b)
t_{ad}	Bondline thickness in Fig. 3(a), (b)
t	Adherend end thickness in Fig. 3(a), (b), $t = 2\,t_1 + t_{ad}$
α, β	Dundurs' material composite parameters defined in Eq. (2).
θ_{ol}, θ_{or}	Deformation angles at the interface corner O
θ_C	Deformation angle at the interface corner C
λ	Singular index obtained from eigenequation (1)
σ_y, τ_{xy}	Tension and shear stress component near the interface end (see Fig. 3)
σ_o	Tension stress at both ends of single lap joint
σ_c	Adhesive strength
τ_{ave}	Average shear stress at fracture
ν	Poisson's ratio
W	Joint width

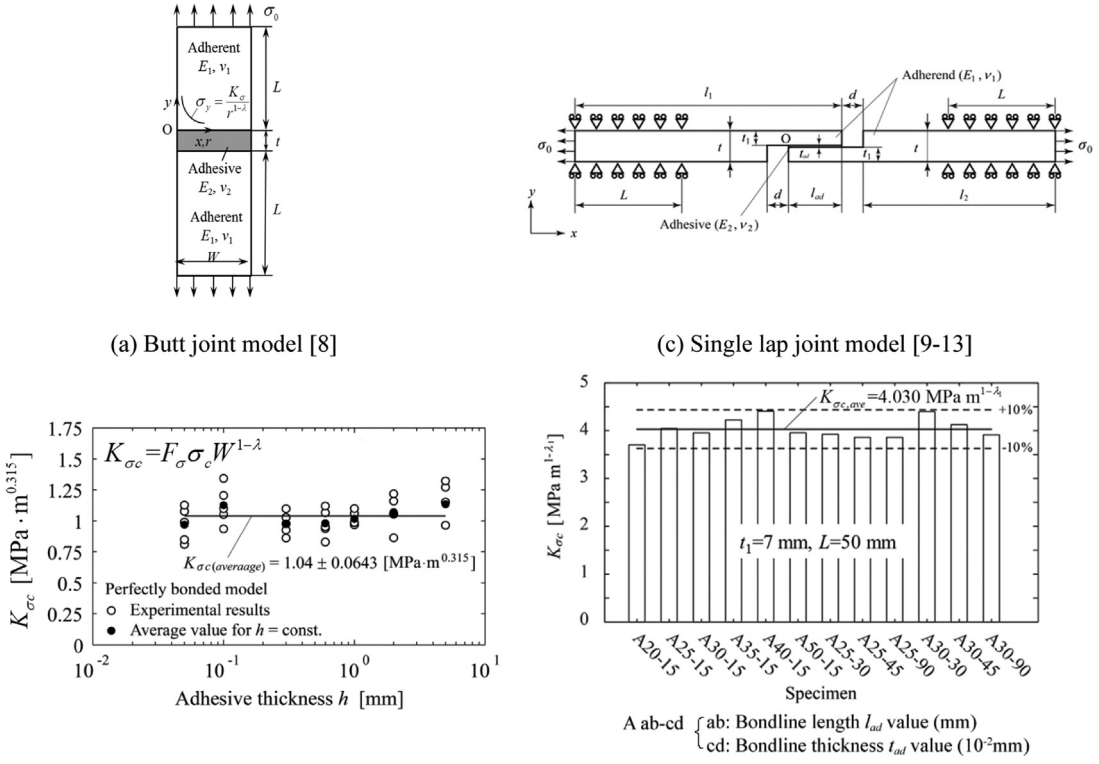

(a) Butt joint model [8]

(c) Single lap joint model [9-13]

(b) Adhesive strength of butt joint [8]

(d) Adhesive strength of single lap joint [9-13]

Fig. 1. Adhesive strength expressed as a constant value of the critical ISSF $K_{\sigma c}$ = const.

be found in [9–13]. The singular stress field for lap joints is characterized by the singular index λ, which can be determined from eigenequation (1) [22–24]. As shown in Appendix A, Eq. (1) has two real roots for most of the material combinations.

$$\begin{aligned} &4\sin^2(\pi\lambda)\left\{\sin^2\left(\frac{\pi\lambda}{2}\right)-\lambda^2\right\}\beta^2+4\lambda^2\sin^2(\pi\lambda)\,\alpha\beta\\ &+\left\{\sin^2\left(\frac{\pi\lambda}{2}\right)-\lambda^2\right\}\alpha^2-4\lambda^2\sin^2(\pi\lambda)\,\beta\\ &-2\left\{\lambda^2\cos(2\pi\lambda)+\sin^2\left(\frac{\pi\lambda}{2}\right)\cos(\pi\lambda)+\frac{1}{2}\sin^2(\pi\lambda)\right\}\alpha\\ &+\sin^2\left(\frac{3\pi}{2}\lambda\right)-\lambda^2=0 \end{aligned} \tag{1}$$

Here, α and β are Dundurs' parameters [25] defined by Poisson's ratio ν_m and shear modulus G_m(m = 1 is for adhesive, m = 2 is for adherend).

$$\alpha = \frac{G_1(\kappa_2+1)-G_2(\kappa_1+1)}{G_1(\kappa_2+1)+G_2(\kappa_1+1)},\quad \beta = \frac{G_1(\kappa_2-1)-G_2(\kappa_1-1)}{G_1(\kappa_2+1)+G_2(\kappa_1+1)},$$
$$\kappa_m = \begin{cases} \frac{3-\nu_m}{1+\nu_m}(\text{plane stress}) \\ 3-4\nu_m(\text{plane strain}) \end{cases} (m = 1,\ 2). \tag{2}$$

Since the previous studies showed that the adhesive strength can be expressed as a constant value of the ISSF in 2D modelling [8–13], this study will discuss the effect of the specimen geometry on the ISSF. Table 1 shows the elastic parameters of the adherend and adhesive for the specimen used by Park et al. [21]. Fig. 3 shows two types of lap joint modelling by extending the specimen used in [21] with fixed bondline length l_{ad} = 25 mm, fixed bondline thickness l_{ad} = 25 mm under the load parameter $P/W = \sigma_o t$ = 14.15 N/mm. Here, the load parameter $P/W = \sigma_o t$ = 14.15 N/mm is corresponding to tensile stress σ_o = 1 MPa in Park's specimen having the dimension $t = 2\,t_1 + t_{ad} = (2 \times 7 + 0.15)$

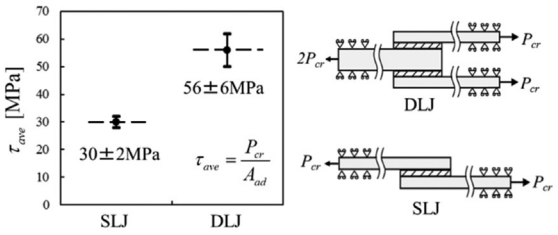

(a) Critical average shear stress obtained by single lap joint (SLJ) and double lap joint (DLJ) when the adherend is S45C and the adhesive is epoxy [19, 20]

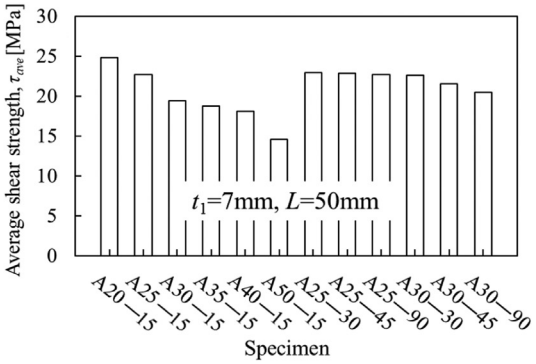

(b) Critical average shear stress experimentally obtained leading to the results in Fig.1(b) by varying bondline dimensions l_{ad} =20-50mm and t_{ad} =0.15-0.90mm when the adherend is aluminum alloy and the adhesive is epoxy [21]

Fig. 2. Adhesive strength expressed as an average shear stress.

= 14.15 mm and W = 25 mm [21]. The total length of the specimen in Fig. 3 is 225 mm with d = 10 mm. In Fig. 3(a), the adherend thickness t_1 and fixed boundary length L are mainly changed. In Fig. 3(b), the tensile direction is mainly changed with the distance e.

The stresses σ_y and τ_{xy} around the interface end can be expressed as follows. The notation r denotes the radial distance away from the corner singular point O.

$$\sigma_y = \frac{K_{\sigma,\lambda_1}}{r^{1-\lambda_1}} + \frac{K_{\sigma,\lambda_2}}{r^{1-\lambda_2}} \cong \frac{K_{\sigma,\lambda_1}}{r^{1-\lambda_1}}(1 + C_\sigma\, r^{\lambda_2-\lambda_1}),$$
$$\tau_{xy} = \frac{K_{\tau,\lambda_1}}{r^{1-\lambda_1}} + \frac{K_{\tau,\lambda_2}}{r^{1-\lambda_2}} \cong \frac{K_{\tau,\lambda_1}}{r^{1-\lambda_1}}(1 + C_\tau\, r^{\lambda_2-\lambda_1}).$$
$$C_\sigma = K_{\sigma,\lambda_2}/K_{\sigma,\lambda_1},\ \ C_\tau = K_{\tau,\lambda_2}/K_{\tau,\lambda_1}. \tag{3}$$

Here, K_{σ,λ_1} and K_{σ,λ_2} denote the ISSFs. The previous studies showed that the ratios $C_\sigma = K_{\sigma,\lambda_2}/K_{\sigma,\lambda_1}$ and $C_\tau = K_{\tau,\lambda_2}/K_{\tau,\lambda_1}$ are almost constants except for extreme adhesive geometry [8–13]. The effects of $K_{\sigma,\lambda_2}/r^{1-\lambda_2}$ and $K_{\tau,\lambda_2}/r^{1-\lambda_2}$ in Eq. (3) may be very small since $\lambda_2 \approx 1$. Also it is known that K_{σ,λ_1} and K_{τ,λ_1} are expressed by a single ISSF parameter [9–13], and therefore, both ISSFs in Eq. (3) can be controlled by K_{σ,λ_1} alone.

In this study, the reference solution is denoted by K^*_{σ,λ_1} and the unknown solution is denoted by K_{σ,λ_1}. Then, FEM stresses obtained by the finite element method (FEM) are denoted by $\sigma^*_{y0,\mathrm{FEM}}$ for the reference solution and $\sigma_{y0,\mathrm{FEM}}$ for unknown problem. Thus, from Eq. (3), the relation between $K_{\sigma,\lambda_1}/K^*_{\sigma,\lambda_1}$ and $\sigma_{y0,\mathrm{FEM}}/\sigma^*_{y0,\mathrm{FEM}}$ can be expressed as follows.

$$\frac{K_{\sigma,\lambda_1}}{K^*_{\sigma,\lambda_1}} = \frac{\sigma_{y0,\ \mathrm{FEM}}}{\sigma^*_{y0,\ \mathrm{FEM}}} \tag{4}$$

If the reference ISSF K^*_{σ,λ_1} is available, K_{σ,λ_1} can be obtained from the FEM stress ratio by applying the same mesh pattern to the reference problem [8–13]. In Eq.(4), the reference solution K^*_{σ,λ_1} can be obtained by using the Reciprocal Work Contour Integral Method (RWCIM). The detail information of the calculation process and the exact value of the reference solution K^*_{σ,λ_1} were presented in [13]. Then, K_{σ,λ_1} can be obtained from the FEM stress ratio by applying the same mesh pattern to the reference problem.

Table 2 shows the singular indexes λ_1, λ_2 for several material combinations considered in [26,27] including stainless steel SUS304, aluminum alloy A7075, silicon and IC substrate FR-4.5 as the adherends with resin as the adhesive. It is found that the weaker singular index λ_2 = 0.9914~0.9999 ≈ 1, which is close to no singularity as λ_2 = 1.

Fig. 4 shows λ_2 values on (α, β) map for all material combinations. In Fig. 4, open circles (○) denote the results for several metals-resin combinations. All metal-resin combinations are in the range E_1 = 108.4 – 206 GPa, ν_1 = 0.249 – 0.300, E_2 = 0.037 – 3.6 GPa, ν_2 = 0.294 – 0.498. Then, it is seen that all open circle marks are in the range λ_2 = 0.99–1. Since always $\lambda_2 \approx 1$, the present method may be useful for evaluating all metal-resin lap joints.

Fig. 5 shows an example of FEM mesh around the interface end. The linear elastic analyses are performed under the plane strain condition by using the software MSC Marc. The element types chosen are quad 4 and quad 8. Here, 8-node elements are used in the vicinity of the interface end, 4-node elements are used in other regions. The minimize element size around the corner $e_{\min}$ is 3^{-12} mm. Note that the mesh-independent technique used in this study 4-node element is enough and 8-node element is not necessary since the FEM error can be eliminated by using the FEM ratio. However, 8-node elements are more convenient to obtain the reference solution by calculating the path integrals in RWCIM [9–13].

As shown in Fig. 6, the bend deformation can be described by focusing on the deformation angle θ_C at the interface end C. The detail information for the deformation angle θ_C is indicated in Appendix B. In this study, the deformation angle θ_C at the interface end C is determined from Point C and Point D with distance l_θ. Table 3 shows the effect of l_θ

Table 1
Material properties of adherend and adhesive.

Materials		Young's modulus E [GPa]	Poisson's ratio ν	α	β	λ_1	λ_2
Adherend	Aluminum alloy 6061-T6	68.9	0.3	-0.8699	-0.06642	0.6062	0.9989
Adhesive	Epoxy resin	4.2	0.45				

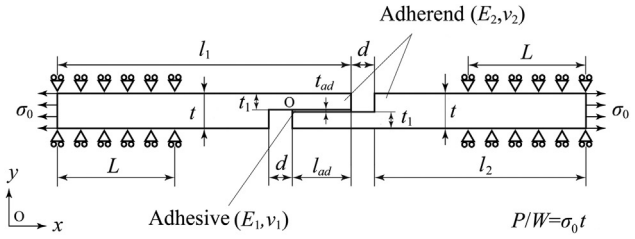

(a) Lap joint model where the adherend thickness t_1 and fixed boundary length L are mainly changed with fixed dimensions l_{ad}=25mm and t_{ad}=0.15mm under $P/W=\sigma_o t$ =14.15N/mm

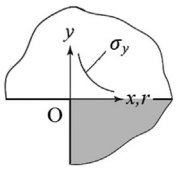

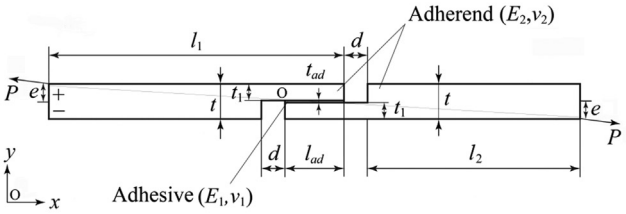

(b) Lap joint model where the tensile direction is mainly changed with fixed dimensions l_{ad}

Fig. 3. Analysis model and boundary condition.

Table 2
Singular indexes for single lap joint with different material combinations.

	Material	Young's modulus E [GPa]	Poisson's ratio ν	λ_1	λ_2
Adherend	SUS304(stainless steel)	206	0.3	0.6568	0.9999
	A7075(aluminum alloys)	71	0.33	0.6489	0.9995
	Silicon	166	0.26	0.6552	0.9999
	FR-4.5(IC substrate)	15.34	0.15	0.6020	0.9914
Adhesive	Resin	2.74	0.38		

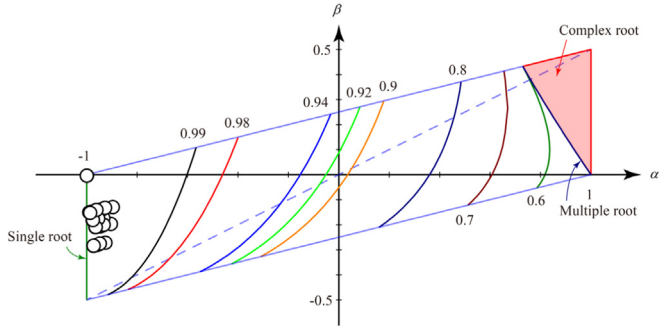

○ λ_2 for the material combinations of metals (E_2 = 108.4 ~ 206 GPa, ν_2 = 0.249 ~ 0.300) and adhesives (E_1 = 0.037 ~ 3.6 GPa, ν_1 = 0.294 ~ 0.498) which are generally used in adhesive joints

Fig. 4. Values of singular index λ_2 on (α, β) map.

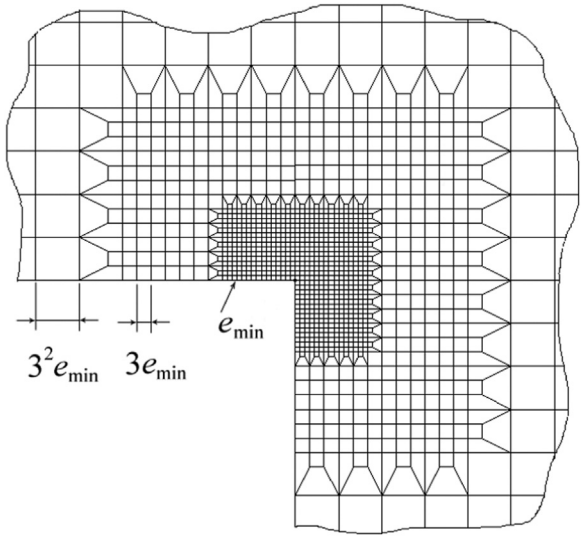

Fig. 5. Mesh pattern around the interface end.

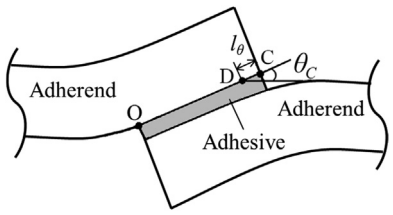

Fig. 6. Deformation near the interface end.

on θ_C by varying the minimum mesh size e_{min} by taking an example of t_1 = 7 mm, L = 50 mm and l_2 = 90 mm. Due to the singular stress field around the interface end, the θ_C value varies depending on l_θ. In Table 3 it is seen that θ_C is insensitive to minimum mesh size e_{min}. Therefore, in this study, the maximum value of θ_C is used to discuss the bend deformation. The l_θ value giving the maximum θ_C is depending on the interface end shape and material combination. In Table 3, the maximum value of θ_C appears at $l_\theta = 1/3^3$mm independent of the minimum

Table 3
Deformation angle θ_C with varying $e_{\min}$ and l_θ.

l_θ[mm]	θ_C		
	$e_{\min} = 1/3^{11}$mm	$e_{\min} = 1/3^{8}$ mm	$e_{\min} = 1/3^{5}$ mm
$1/3^4$	0.0186	0.0188	0.0187
$1/3^3$	0.0194	0.0194	0.0194
$1/3^2$	0.0188	0.0188	0.0188
1/3	0.0162	0.0162	0.0162

(a) With fillet (adhesive geometry in experiments) (b) Without fillet (analysis model in this study)

Fig. 7. Fillet at bonded edge.

mesh size $e_{\min}$. The reason why θ_C has a peak value near $l_\theta = 0$ is explained in Appendix B.

In lap joint specimens experimentally used, adhesive fillets may exist at the bonded ends as shown in Fig. 7(a). In this study, the local geometry as shown in Fig. 5 has been assumed. If the local geometry is changed by the fillet, the singular stress field and the singular index are changed. Then, the adhesive strength evaluation becomes difficult. FEM analysis has shown that the stress concentration may decrease at the interface end by introducing the fillets [28]. However, Arai and Kobayashi [29] have shown that the debonding of the fillet occurs when the load is smaller than the final fracture. They have concluded that the specimens with and without fillet in Fig. 7(a), (b) have nearly the same strength. Similarly, Campilho, Moura and Domingues have analyzed the effect of the fillet geometries on the strength [30]. They have reported that the modelling validity is confirmed experimentally and the strength in Fig. 7(a) is just slightly larger than the strength in Fig. 7(b). Since those previous studies show that the fillet effect in Fig. 7(a) is not very large, the authors think that the ISSF modelling as shown in Fig. 7(b) can be applied to other adhesive geometries including fillet. This might be analogous to continuing use of the SIFs (Stress Intensity Factors) in crack problems even though the small scale yielding is violated.

3. Pure shear testing to minimize ISSF and bend effect

In this section, the most suitable lap joint testing is investigated to minimize bend effect in terms of the ISSF under the same magnitude of load $P/W = 14.15$ N/mm ($\sigma_o = 1$MP when $t = 14.15$ mm). In simulation process, the fixed boundary length L and the adherend thickness t_1 in Fig. 3(a) and loading direction in Fig. 3(b) will be changed under fixed $l_{ad} = 25$ mm and $t_{ad} = 0.15$ mm. The effects of bondline length l_{ad} and bondline thickness t_{ad} were studied previously [9–13] (see Appendix C). The material combination is also fixed as shown in Table 1 since the ISSF should be compared under the same singular index λ_1 and λ_2.

First, a special case is considered as shown in Fig. 8 to obtain the minimum value of ISSF $K_{\sigma,\lambda_1} = K_{\sigma,\min}$. In Fig. 8(a), t_1 is changed when the adherends are fixed along the whole boundary ($L = l_1$ or l_2 in Fig. 3(a)) for the fixed dimensions of $l_{ad} = 25$ mm and $t_{ad} = 0.15$ mm under the load $P/W = \sigma_o t = 14.15$ N/mm. Note that appropriate dimensionless expression for Fig. 8 is difficult since the lap joint in Fig. 3 has a complicated form. For butt joint specimen in Fig. 1(a), the dimensionless factors to control the ISSF have been clarified in the recent study [31]. In Fig. 8, with increasing adherend thickness t_1, the K_{σ,λ_1} decreases initially and then slightly increases, and finally becomes almost constant when t_1 is large enough. The minimum ISSF $K_{\sigma,\min} = 0.0422\text{MPa}\cdot\text{m}^{1-\lambda_1}$ can be obtained when $t_1 = 13$ mm.

Fig. 8(b) shows the minimum deformation angle $\theta_C = \theta_{C,\min}$. With increasing the adherend thickness t_1, the deformation angle θ_C first decreases, then increases slightly and finally becomes constant when t_1 is large enough. The minimum angle $\theta_{C,\min} = 0.0042$ degree can be obtained when $t_1 = 13$ mm.

Fig. 9(a) shows the results for fixed boundary length $L = 50$ mm, 80 mm, 90 mm. Here, the notation JIS* denotes the results of JIS K6850 prescribing the adherend thickness $t_1 = 1.5$ mm and $L = 50$ mm. The dashed line shows the minimum ISSF value $K_{\sigma,\min} = 0.0422\text{MPa}\cdot\text{m}^{1-\lambda_1}$. With increasing t_1, the ISSF K_{σ,λ_1} decreases and becomes constant when t_1 is large enough. When $t_1 \geq 25$ mm, the effect of L can be ignored. The value $K_{\sigma,\lambda_1}|_{t_1=1.5\text{mm}} = 0.2270\text{MPa}\cdot\text{m}^{1-\lambda_1}$ of JIS K6850 is 5 times larger than the value of $K_{\sigma,\min}$. The value of Park's specimen [21] $K_{\sigma,\lambda_1}|_{t_1=7\text{mm}} = 0.1010\text{MPa}\cdot\text{m}^{1-\lambda_1}$ is still more than twice larger than $K_{\sigma,\min} = 0.0422\text{MPa}\cdot\text{m}^{1-\lambda_1}$. The results show that the specimen [21] is much better than the JIS to obtain the adhesive strength, but still insufficient to obtain $K_{\sigma,\min} = 0.0422\text{MPa}\cdot\text{m}^{1-\lambda_1}$. An international standard ASTM D5656 specifies the adhesive adherend thickness 9.53 mm for pure shear strength characterization. Fig. 9 shows that adherend thickness $t_1 = 9.53$ mm is much better than the one of JIS specimens, but still insufficient to obtain the minimum ISSF.

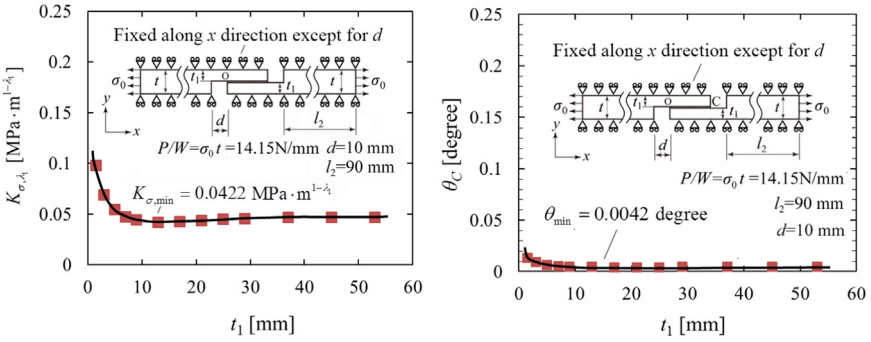

(a) ISSF K_{σ,λ_1} (b) Deformation angle θ_C

Fig. 8. Effect of adherend thickness t_1 when $L =$ the whole boundaries ($= l_1$ or l_2) for fixed dimensions $l_{ad} = 25$ mm and $t_{ad} = 0.15$ mm in Fig. 3(a) under $P/W = \sigma_o t = 14.15$ N/mm.

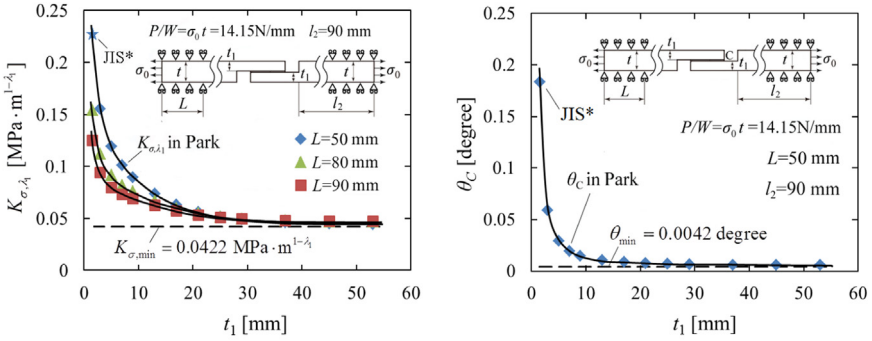

(a) ISSF K_{σ,λ_1} (b) Deformation angle θ_C

Fig. 9. Effects of adherend thickness t_1 when L = 50, 80, 90 mm for fixed dimensions l_{ad} = 25 mm and t_{ad} = 0.15 mm in Fi.3 (a) under $P/W = \sigma_0 t$ = 14.15 N/mm (JIS*: JIS K6850 prescribes specimen when t_1 = 1.5 mm, L = 50 mm).

Fig. 9(b) shows the results of deformation angle θ_C when L = 50 mm since in most of the previous experiments $L \cong$ 50 mm. Fig. 9(b) shows θ_C decreases rapidly and then become constant with increasing t_1. The minimum θ_C expressed as the dashed line can be obtained when t_1 is large enough. The value $\theta_C|_{t1=1.5mm}$ = 0.1834 degree of JIS specimen is about 40 times larger than the minimum angle $\theta_{C,\min}$. The value $\theta_C|_{t1=7mm}$ = 0.0193 degree of Park [21] is about 4 times larger than that the minimum angle $\theta_{C,\min}$. It is seen that the specimen in [21] is much better than the JIS, but insufficient to obtain the minimum value $\theta_{C,\min}$ = 0.0042 degree.

Fig. 10(a) shows the effect of adherend length l_2 on the ISSF K_{σ,λ_1} when t_1 = 7 mm and L = 50 mm in Fig. 3(a). Only in Fig. 10, the total specimen length is changed as 145~335 mm by changing l_2 but in other figures the total length is always fixed as 225 mm. The dashed line shows the minimum value $K_{\sigma,\min}$ = 0.0422MPa·m$^{1-\lambda_1}$ when t_1 = 53 mm. When t_1 = 7 mm, with increasing adherend length l_2, the ISSF K_{σ,λ_1} increases. However, when t_1 = 53 mm, the K_{σ,λ_1} is almost constant. In other words, the effect of adherend length l_2 can be ignored when t_1 is large enough. This is because the large adherend thickness may eliminate bending effect since the adherend becomes rigid enough. It may be concluded that K_{σ,λ_1} can be minimized by using small l_2 and large t_1.

Fig. 10(b) shows the results of deformation angle θ_C when t_1 = 7 mm. The dashed line shows the minimum value $\theta_{C,\min}$ = 0.0042degree when t_1 = 53 mm. With increasing l_2, θ_C increases for t_1 = 7 mm, but θ_C is almost constant for t_1 = 53 mm. When t_1 is large enough, the minimum $\theta_{C,\min}$ = 0.0042 degree can be obtained easily since the effect of l_2 on θ_C can be ignored.

As mentioned in Section 2, the previous study showed C_σ and C_τ in Eq. (3) are almost constant independent of adhesive geometry. In a similar way, Fig. 11 shows the effect of adherend geometry on C_σ and

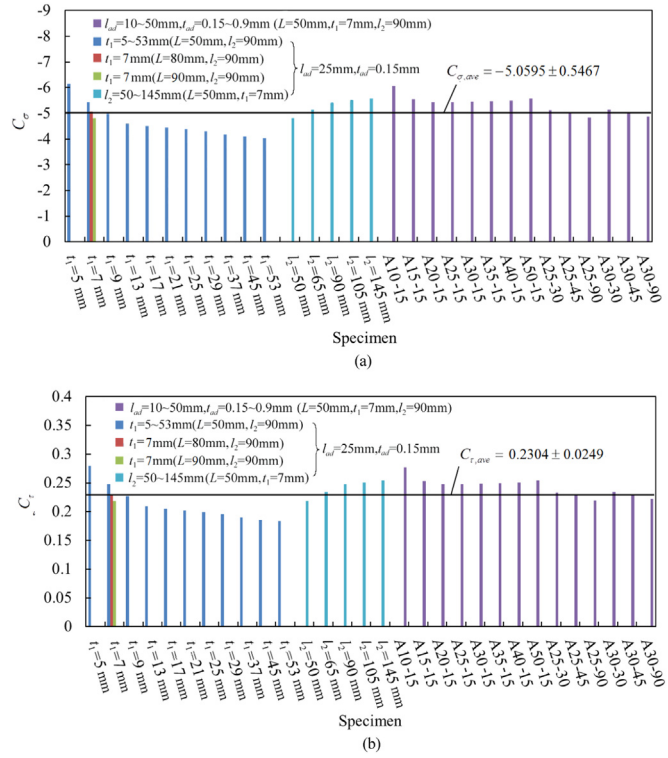

Fig. 11. (a) Results of C_σ for single lap joint with different specimen geometries, (b) Results of C_τ for single lap joint with different specimen geometries.

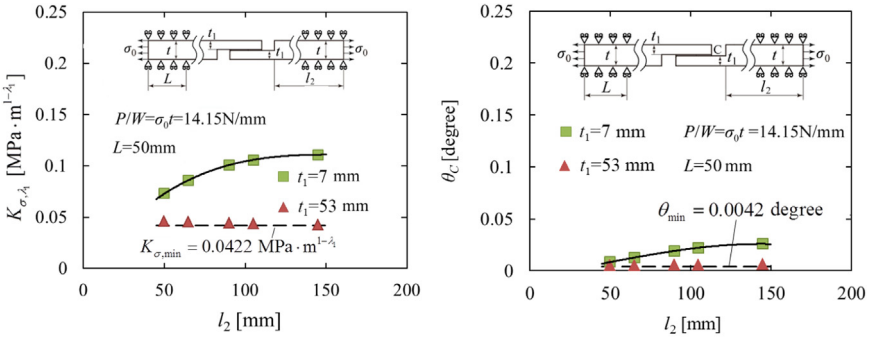

(a) ISSF K_{σ,λ_1} (b) Deformation angle θ_C

Fig. 10. Effects of adherend length l_2 on K_{σ,λ_1} when t_1 = 7, 53 mm and L = 50 mm in Fig. 3(a) under fixed l_{ad} = 25 mm, t_{ad} = 0.15 mm and $P/W = \sigma_0 t$ = 14.15 N/mm (In Fig. 10, the total length of the specimen is changed as 145~335 mm, in other Figures the total length is always fixed as 225 mm.

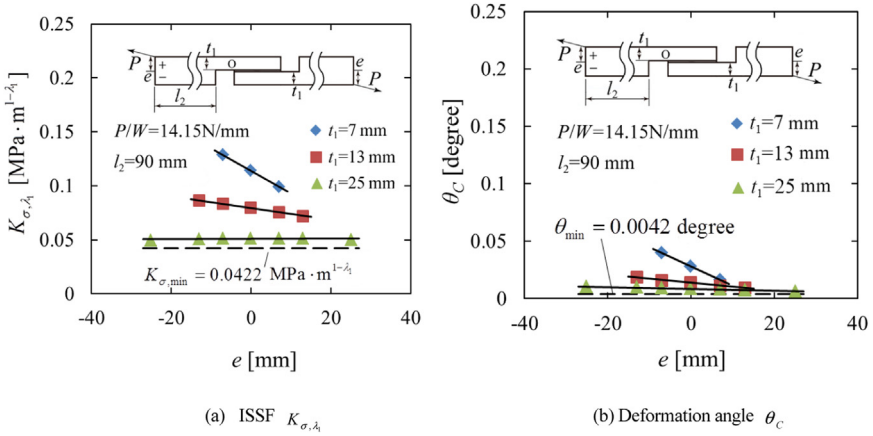

Fig. 12. Effects of distance e when and adherend thickness t_1 = 7, 13, 25 mm in Fig. 3(b) under fixed l_{ad} = 25 mm, t_{ad} = 0.15 mm and P/W = 14.15 N/mm.

C_τ. In Fig. 11, C_σ and C_τ values are indicated by varying l_{ad} = 10~50 mm, t_{ad} = 0.15~0.9 mm, t_1 = 5~53 mm, l_2 = 50~145 mm, L = 50~90 mm in Fig. 3(a). From Fig. 11, we have C_σ = -5.0595 ± 0.5467, C_τ = 0.2304 ± 0.0249. The variations of C_σ and C_τ are small except for the cases of small adherend thickness. For example, for small adherend thickness t_1 = 1.5 and t_1 = 3 mm, we have $C_\sigma|_{t1=1.5mm}$ = -9.8942, $C_\sigma|_{t_1=3mm}$ = -7.4799, $C_\tau|_{t_1=1.5mm}$ = 0.4505, $C_\tau|_{t_1=3mm}$ = 0.3406 even other geometries are the same as l_{ad} = 25 mm, t_{ad} = 0.15 mm, l_2 = 90 mm, L = 50 mm. This large discrepancy between small and large thickness specimens can be explained from the difference of the bend deformation.

Fig. 12(a) shows the relationship between the ISSF K_{σ,λ_1} and the eccentric distance e in Fig. 3(b). It is found that the K_{σ,λ_1} decreases with increasing the positive distance e. The effect of e on K_{σ,λ_1} becomes larger when the adherend thickness is smaller as t_1 = 7 mm. When t_1 = 25 mm, K_{σ,λ_1} is almost constant independent of e.

Fig. 12(b) shows the relationship between deformation angle θ_C and eccentric distance e in Fig. 3(b). It is found that θ_C decreases with increasing e. The effect of e on θ_C is significant when the adherend thickness is small when t_1 = 7 mm. When t_1 = 25 mm, θ_C is almost constant independent of e.

4. Relationship between ISSF and deformation angle at the interface corner

As shown in Fig. 8–10 and Fig. 12, similar variations can be seen for ISSF K_{σ,λ_1} and deformation angle θ_C. Fig. 13 shows the relation between K_{σ,λ_1} and θ_C by using all results discussed in Section 3. As can be seen from Fig. 13, K_{σ,λ_1} is controlled by θ_C uniquely and K_{σ,λ_1} decreases with decreasing θ_C. In other words, K_{σ,λ_1} variation can be explained by θ_C and similarly θ_C variation can be explained by K_{σ,λ_1}. As an example, when adherend thickness t_1 = 1.5 mm prescribed by JIS, both K_{σ,λ_1} and θ_C are very large. The minimum K_{σ,λ_1} and θ_C can be obtained when the adherend thickness t_1 is large enough as $t_1 \geq$ 25 mm. It is seen that the bend effect is minimized when $t_1 \geq$ 25 mm. The reason why the minimum $K_{\sigma,\lambda_1} \neq 0$ can be explained by $\theta_C \neq 0$ due to the local bend deformation at the interface end, which can be observed even for very large thickness. Therefore, the bend effect in single lap joint can be minimized when the adherend thickness is large enough.

5. How to obtain the adhesive strength for double lap joint by using single lap joint

The experimental results show that the strength of DLJ is about two times larger than the strength of SLJ as shown in Fig. 14(a) [19]. However, the critical ISSF $K_{\sigma c}$ is the same for the double and single lap joints as shown in Fig. 14(b). In this section, therefore, the equivalent strength conditions for the SLJ on the DLJ in Fig. 15 will be considered in terms of the ISSF K_{σ,λ_1} by varying the adherend thickness t_1. In addition, since end tabs are often used by bonding at the ends of experimental specimens to reduce bend effect when loaded, the influence of the tab on K_{σ,λ_1} will be also considered. Here, the same material of the adherend is assumed for the tab.

As shown in Fig. 15(a), (b) for the SLJ, both interface corners can be

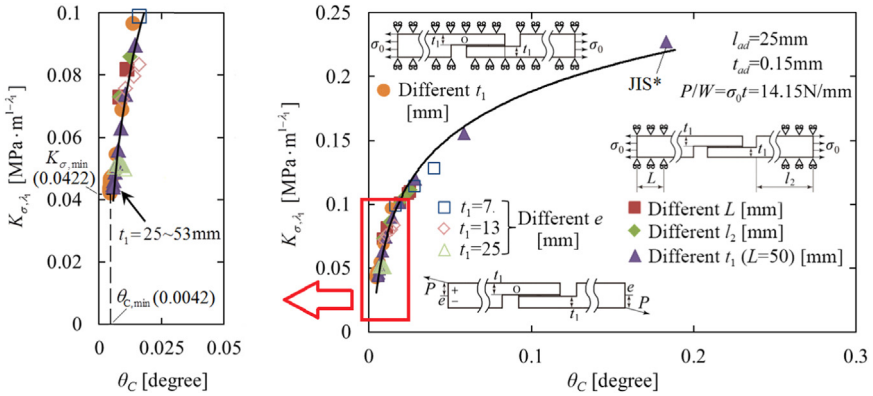

Fig. 13. Unique relationship between K_{σ,λ_1} and θ_C.

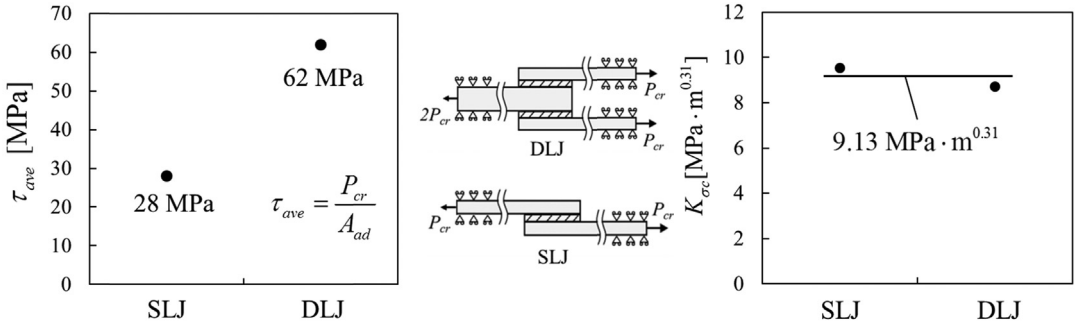

(a) Average shear strengths of SLJ and DLJ

(b) The critical ISSF $K_{\sigma c}$ of SLJ and DLJ

Fig. 14. Adhesive strength of single lap joint (SLJ) and double lap joint (DLJ) (Adherend: S45C, Adhesive: Epoxy B).

denoted as point "O_1" because of the symmetry. However, as shown in Fig. 15(c), (d) for the DLJ, since the ISSFs at the interface corners are different, they are denoted by corner "O_1" and corner "O_2".

Fig. 16 shows the results of ISSF K_{σ,λ_1} at interface corners O_1 and O_2. It is found that the K_{σ,λ_1} at corner O_1 is larger than that at corner O_2. The K_{σ,λ_1} for the specimen with tab is nearly equal to the K_{σ,λ_1} for the specimen without tab. Therefore, the fracture may occur at corner O_1 during testing. For this reason, the equivalent conditions of strength for SLJ and DLJ will be considered by using the K_{σ,λ_1} at interface corner O_1.

Fig. 17 shows the ISSFs K_{σ,λ_1} at interface corner O_1 by varying the

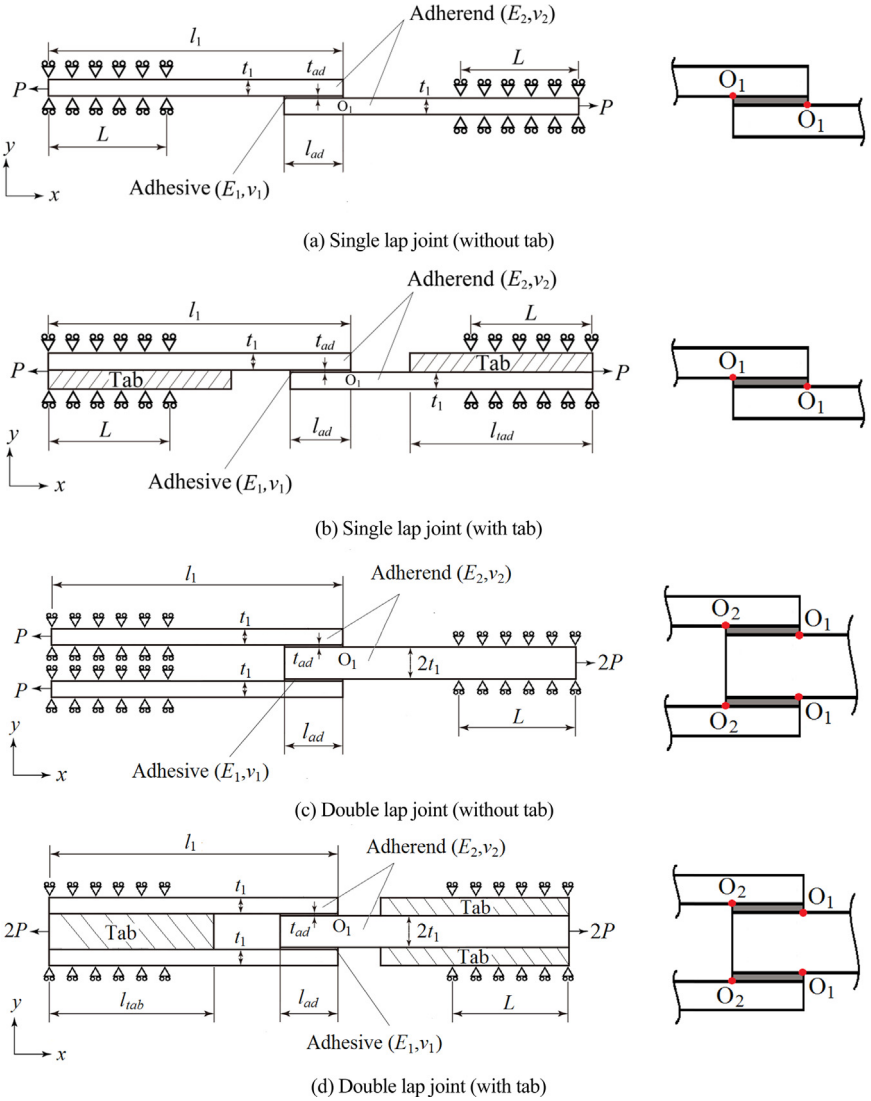

(a) Single lap joint (without tab)

(b) Single lap joint (with tab)

(c) Double lap joint (without tab)

(d) Double lap joint (with tab)

Fig. 15. Analysis models of lap joints.

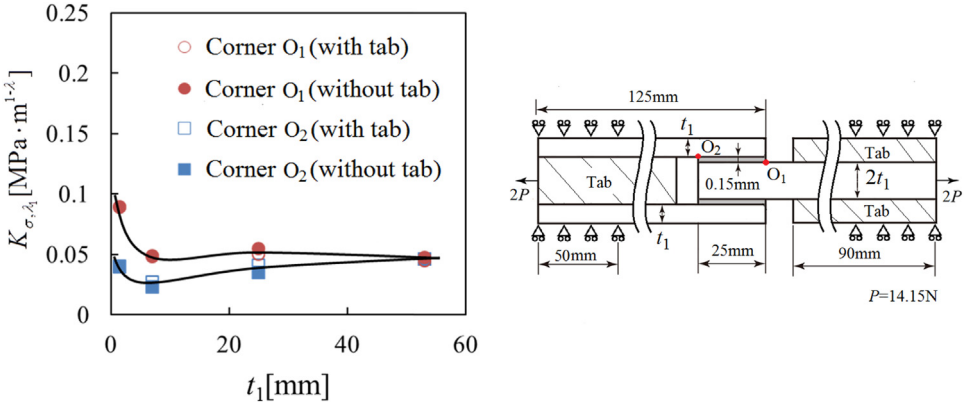

Fig. 16. ISSF K_{σ,λ_1} for double lap joint (see Fig. 15(c),(d)).

adherend thicknesses t_1 for both single and double lap joints. Both ISSFs decrease with increasing adherend thickness t_1. When $t_1 \geq 25$ mm, both ISSFs become constant independent of t_1. In JIS, the adherend thickness is prescribed as $t_1 = 1.5$ mm. The K_{σ,λ_1} of the SLJ with $t_1 = 7$ mm is nearly equal to the K_{σ,λ_1} of the DLJ with $t_1 = 1.5$ mm (JIS). Similarly, the K_{σ,λ_1} of the SLJ is nearly equal to the K_{σ,λ_1} of the DLJ when $t_1 \geq 25$ mm. By using those geometries the same adhesive strength can be obtained for SLJ and DLJ.

When adherend thickness $t_1 \geq 25$ mm, the minimum ISSF $K_{\sigma,\min}$ can be obtained as $K_{\sigma,\min} = 0.0422\text{MPa}\cdot\text{m}^{1-\lambda_1}$. Under this condition, the bend effect can be minimized. The reason why $K_{\sigma,\min} \neq 0$ can be explained from slight local deformation observed at the interface end. The deformations of the lap joints in Fig. 17 without tab are shown in Fig. 18 where the deformation is magnified by 300 times. As can be seen from Fig. 18, when $t_1 = 1.5$ mm, the bend deformation of the SLJ in Fig. 18(a) is much large than the one of the DLJ in Fig. 18(b). Instead, the bend deformation of SLJ with $t_1 = 7$ mm in Fig. 18 (c) is nearly same as the bend deformation of DLJ with $t_1 = 1.5$ mm in Fig. 18 (b). When $t_1 \geq 25$ mm, all lap joint deformations are nearly the same, and there is only the local bend deformations for Fig. 18(e)~(h).

6. Conclusion

The lap joint testing was originally designed to investigate the adhesive strength under pure shear loading. However, actually pure shear testing is very difficult to be realized in the experiment because of the bend deformation during testing causing the peeling force appearing at the adhesive region. To reduce the bend effect, this study focused on the ISSF at the interface end in order to minimize the ISSF for lap joints. The conclusions can be summarized in the following way.

(1) The effect of specimen geometry was considered under the same adhesive geometry and the same magnitude of load. The ISSF K_{σ,λ_1} decreases with increasing adherend thickness t_1 and the minimum K_{σ,λ_1} was obtained when the adherend thickness is large enough.
(2) The SLJ strength with the adherend thickness $t_1 = 7$ mm is nearly equal to that of DLJ with $t_1 = 1.5$ mm prescribed in JIS. When the adherend thickness is large enough as $t_1 \geq 25$ mm, the single and double lap joint strength is nearly equal the same.
(3) The relationship between the ISSF K_{σ,λ_1} and deformation angle at the interface corner θ_C was discussed. It was found that the ISSF K_{σ,λ_1} decreases with decreasing θ_C, the minimum deformation angle can be obtained also when the adherend thickness t_1 is large enough. The variation of ISSF can be uniquely controlled from the deformation angle at the interface corner. In other words, the bend effect in lap joints can be minimized when the adherend thickness is large enough.
(4) ThSLJ strength with the adherend thickness $t_1 = 7$ mm is nearly equal to that of double lap joint with $t_1 = 1.5$ mm prescribed in JIS. When the adherend thickness is large enough as $t_1 \geq 25$ mm, the single and double lap joint strength is nearly equal the same.

The previous study indicated that the ISSF is a promising method to predict and analyze the bonding-debonding behaviors [8–13]. The ISSF method shows good conformity with the experimental data as shown in Fig. 1(a), (b) and Fig. 14(b). The final goal of this study is to establish a

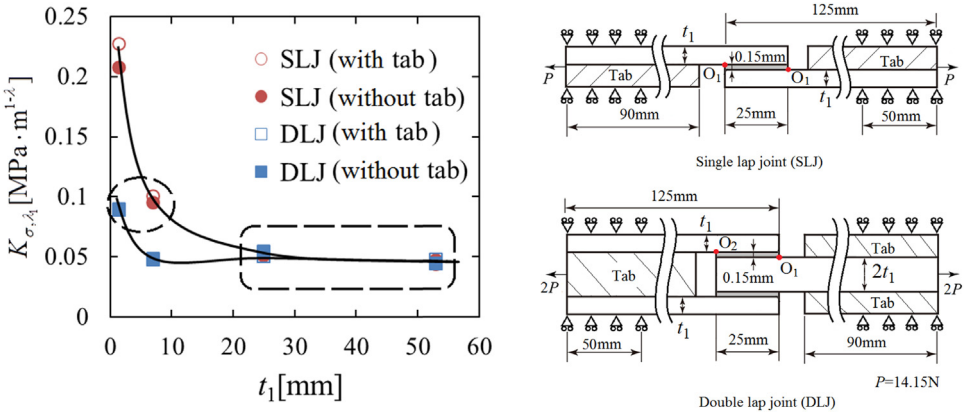

Fig. 17. Comparison of single lap joint (SLJ) and double lap joint (DLJ).

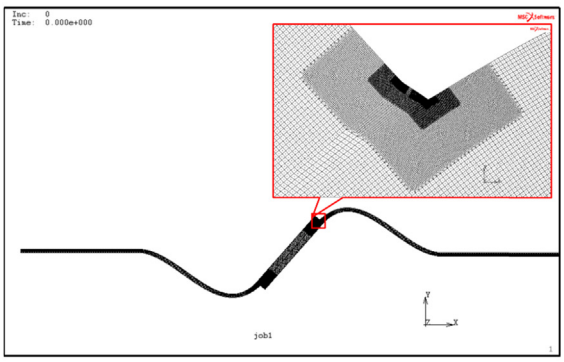

(a) SLJ with t_1=1.5mm

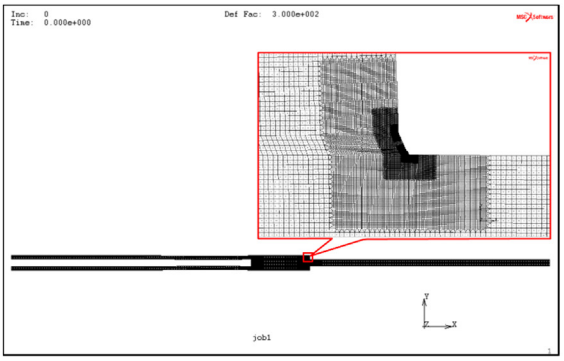

(b) DLJ with t_1=1.5mm

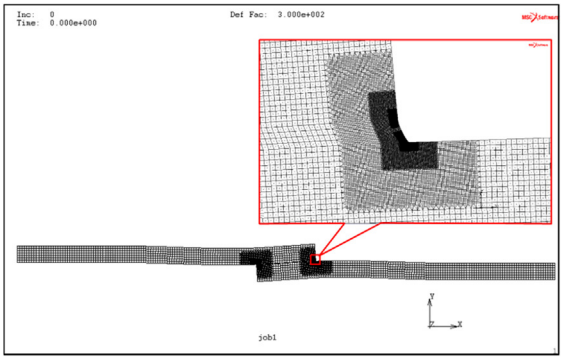

(c) SLJ with t_1=7mm

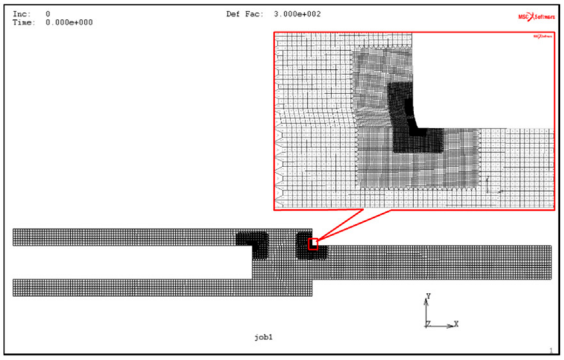

(d) DLJ with t_1=7mm

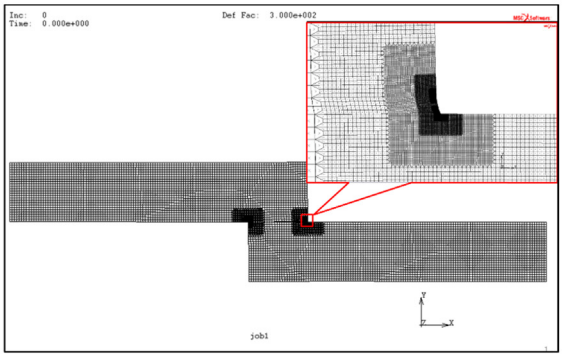

(e) SLJ with t_1=25mm

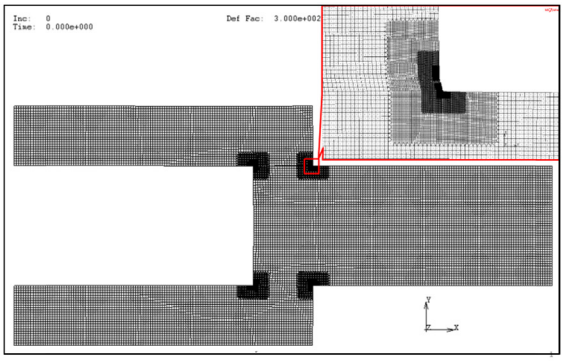

(f) DLJ with t_1=25mm

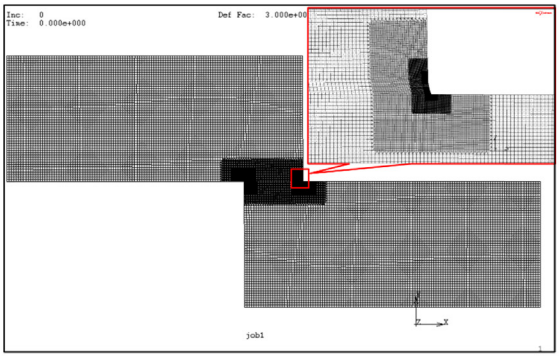

(g) SLJ with t_1=53mm

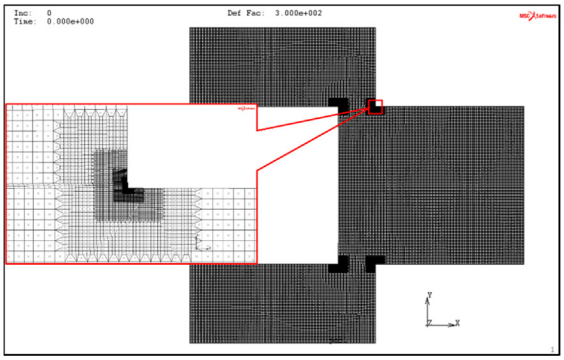

(h) DLJ with t_1=53mm

Fig. 18. Local deformations at the interface end in Fig. 15 (the deformation is magnified by 300 times).

suitable pure shear testing method for adhesive strength by confirming the usefulness experimentally. The authors think that the experimental evidences to support the authors' conclusions can be obtained in future studies since the theoretical background has been indicated in this paper.

Acknowledgement

This study was supported by Japan Society for the Promotion of Science (JSPS) KAKENHI Grant Number JP15K14150.

Appendix A. Singular index for lap joints

Table A.1 shows singular index for lap joints λ within a range of $0 < \mathrm{Re}(\lambda) < 1$, where the underlined figure indicate the multiple root, the bold figure indicate the complex root, the standard style figure indicate the real root. The eigenequation (A.1) has real root, multiple real root or complex root depending on (α, β) except for no root at $(\alpha, \beta) = (-1, -0.5)$. Two real roots appear in most of the material combinations.

Table A.1
Singular index for lap joints $\lambda(0 < \mathrm{Re}(\lambda) < 1)$. [underlined figure indicate multiple root, bold figure indicate complex root, standard style figure indicate real root].

α	$\beta=-0.5$	$\beta=-0.4$	$\beta=-0.3$	$\beta=-0.2$	$\beta=-0.1$	$\beta=0$	$\beta=0.1$	$\beta=0.2$	$\beta=0.3$	$\beta=0.4$	$\beta=0.5$
-1	Non	0.807313	0.720529	0.664609	0.624659	0.594612					
-0.9		0.800102	0.713270	0.657967	0.618663	0.589223					
		0.997323	0.998666	0.999111	0.999333	0.999467					
-0.8		0.794890	0.706604	0.651598	0.612819	0.583934					
		0.988598	0.994363	0.996246	0.997185	0.997748					
-0.7			0.700535	0.645489	0.607116	0.578738					
			0.986584	0.991068	0.993300	0.994638					
-0.6			0.695095	0.639636	0.601547	0.573629	0.552526				
			0.974790	0.983193	0.987375	0.989886	0.991563				
-0.5			0.690364	0.634041	0.596104	0.568599	0.548004				
			0.958485	0.972217	0.979070	0.983201	0.985967				
-0.4			0.686483	0.628716	0.590782	0.563645	0.543552				
			0.937298	0.957761	0.968020	0.974246	0.978436				
-0.3			0.683711	0.623685	0.585580	0.558760	0.539167				
			0.911000	0.939524	0.953867	0.962655	0.968617				
-0.2			0.682542	0.618989	0.580497	0.553941	0.534851	0.521047			
			0.879395	0.917337	0.936302	0.948055	0.956113	0.961997			
-0.1				0.614698	0.575537	0.549184	0.530605	0.517475			
				0.891188	0.915116	0.930101	0.940505	0.948184			
0				0.610930	0.570707	0.544484	0.526433	0.514038			
				0.861179	0.890238	0.908529	0.921385	0.930994			
0.1				0.607894	0.566022	0.539838	0.526433	0.514038			
				0.827429	0.861739	0.883194	0.921385	0.930994			
0.2				0.606003	0.561511	0.535243	0.518343	0.507703	0.501847		
				0.789888	0.829796	0.854095	0.871335	0.884461	0.894894		
0.3					0.557223	0.530697	0.514455	0.504921	0.500526		
					0.794628	0.821357	0.840068	0.854257	0.865522		
0.4					0.553253	0.526195	0.510710	0.502536	0.500000		
					0.756400	0.785186	0.804636	0.819026	0.830167		
0.5					0.549802	0.521736	0.507168	0.500757	0.500737		
					0.715108	0.745794	0.765131	0.778569	0.788128		
0.6					0.547386	0.517317	0.503944	0.500000	0.503736		
					0.670322	0.703330	0.721601	0.732578	0.738354		
0.7						0.512937	0.501301	0.501267	0.511773		
						0.657821	0.673870	0.680168	0.678146		
0.8						0.508591	0.500000	0.508067	0.544319	**0.570579**	
						0.609106	0.621093	0.617814	0.588069	**±0.0645534*i***	
0.9						0.504280	0.504147	**0.532822**	**0.534652**	**0.537138**	
						0.556769	0.558811	**±0.0339893*i***	**±0.072084*i***	**±0.108448*i***	
1						0.500000	**0.500000**	**0.500000**	**0.500000**	**0.500000**	**0.500000**
							±0.0319377*i*	**±0.0645318*i***	**±0.0985231*i***	**±0.134852*i***	**±0.174850*i***

$$
\begin{aligned}
&4\sin^2(\pi\lambda)\left\{\sin^2\left(\tfrac{\pi\lambda}{2}\right)-\lambda^2\right\}\beta^2+4\lambda^2\sin^2(\pi\lambda)\alpha\beta\\
&+\left\{\sin^2\left(\tfrac{\pi\lambda}{2}\right)-\lambda^2\right\}\alpha^2-4\lambda^2\sin^2(\pi\lambda)\beta\\
&-2\left\{\lambda^2\cos(2\pi\lambda)+\sin^2\left(\tfrac{\pi\lambda}{2}\right)\cos(\pi\lambda)+\tfrac{1}{2}\sin^2(\pi\lambda)\right\}\alpha\\
&+\sin^2\left(\tfrac{3\pi}{2}\lambda\right)-\lambda^2=0
\end{aligned}
\tag{A.1}
$$

Appendix B. How to describe the bend deformation of the lap joints

In Appendix B, the bend deformation of the lap joints is presented. Assume that the total length of the specimen is 225 mm, the adhesive length l_{ad} = 25 mm, adhesive thickness t_{ad} = 0.15 mm, fixed boundary length L = 50 mm, adherend length l_2 = 90 mm and P = 14.15 N.

Fig. B.1(a) shows displacements $u_y(x_1)$, $u_y(x_2)$ in the y- direction along the interfaces x_1 and x_2 when the adherend thickness t_1 = 7 mm. As shown in Fig. B.1, displacement $u_y(x_1)$ is skew-symmetric at the centre of the adhesive. Fig. B.1(b) shows the details at the interface end. As can be seen from Fig. B.1(b), small difference 0.000078 mm can be seen at the interface end between $u_y(x_1)$, $u_y(x_2)$.

Fig. B.2 defines several angles to describe the bend deformation. In order to obtain a deformation angle, two target points are considered. Here, l_θ means the distance between the two target points. For the deformation angle θ_{ol} at the interface corner O, the two target points O and A are used. For the deformation angle θ_{or} at the interface corner O, the two target points O and B are used. For the deformation angle θ_C at the interface corner C, two target points C and D are used. The deformation angles θ_{ol}, θ_{or}, θ_C can be defined as follows.

$$
\begin{aligned}
\theta_{or}&=\arctan\left(\frac{y_B-y_O}{x_B-x_O}\right),\\
\theta_{ol}&=\arctan\left(\frac{y_O-y_A}{x_O-x_A}\right),\\
\theta_C&=\arctan\left(\frac{y_C-y_D}{x_C-x_D}\right)
\end{aligned}
\tag{B.1}
$$

Here, x_n and $y_n (n = O,\ A,\ B,\ C,\ D)$ are the coordinates of points O, A, B, C, D.

Fig. B.3(a) shows the results of deformation angles at corner O by varying distances l_θ for t_1 = 7 mm. It is found that both values of θ_{ol} and θ_{or} increase with increasing l_θ, and the difference between θ_{ol} and θ_{or} increases with decreasing l_θ. Therefore, it is not easy to obtain the maximum deformation angle at interface corner O. Fig. B.3(b) shows the results of deformation angle θ_C by varying distances l_θ for t_1 = 7 mm. It is seen that the value of θ_C initially increases and then decreases with increasing l_θ. When the target point D approaches the interface end C beyond a certain limit

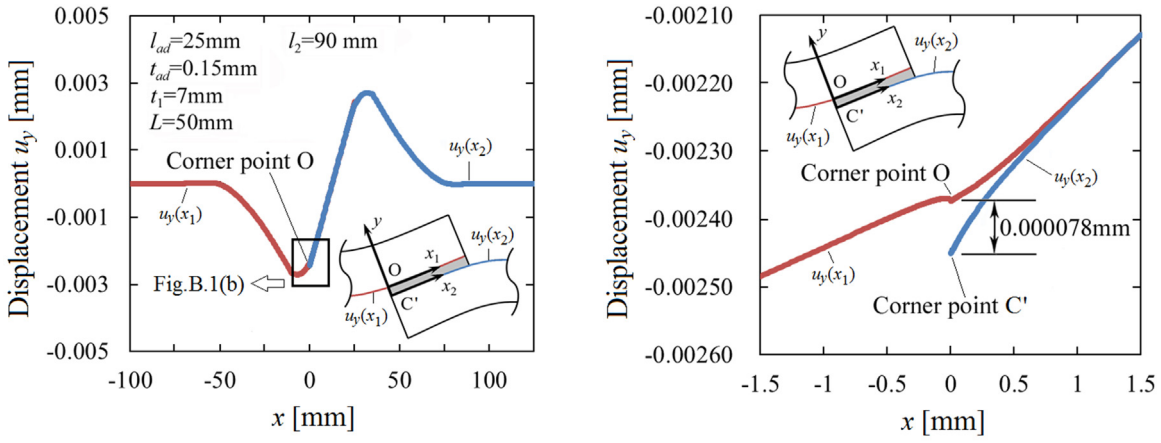

(a) Displacement $u_y(x_1)$ in the range x_1 = -100~25 and Displacement $u_y(x_2)$ in the range x_2 =0~150

(b) Details at the interface ends in Fig.B.1(a)

Fig. B.1. Displacements $u_y(x_1)$, $u_y(x_2)$ in the y-direction along the two interfaces x_1 and x_2.

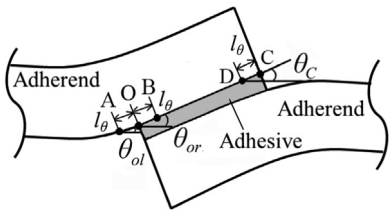

Fig. B.2. Deformation near the interface corner.

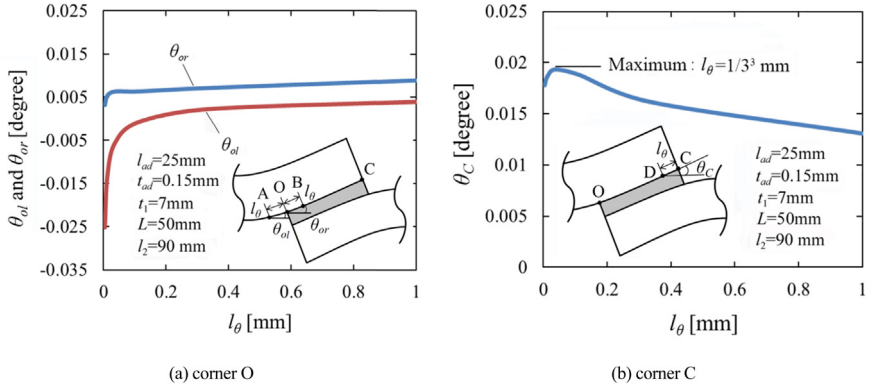

(a) corner O (b) corner C

Fig. B.3. Deformation angle at interface corner edge.

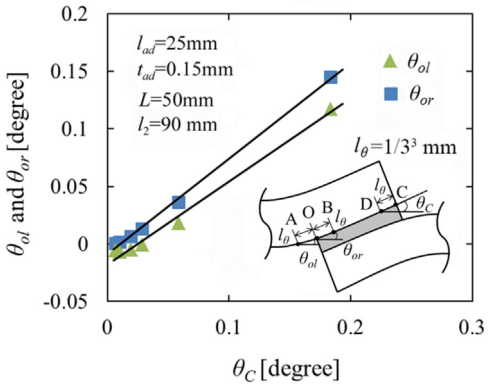

Fig. B.4. Relationship between θ_{ol}, θ_{or} and θ_C.

distance, the increment of (x_C - x_D) becomes larger than the increment of (y_C - y_D) because the interface end C is on a free surface. This is the reason why θ_C becomes smaller when l_θ approaches zero as shown in Fig. B.3(b). As an example shown in Table 3, the maximum θ_C can be obtained when $l_\theta = 1/3^3$ mm independent of element sizes.

Fig. B.4 shows the relationship between deformation angles θ_{ol}, θ_{or} and θ_C. It is found that the θ_C-θ_{ol} relation and θ_C-θ_{or} relation are almost linear, and the slope of the lines are nearly the same. Therefore, in this study, the deformation angle is considered by using the maximum θ_C at corner C.

Appendix C. Effects of the bondline length and bondline thickness on the ISSF

In this study, under the fixed bondline dimensions l_{ad} = 25 mm, t_{ad} = 0.15 mm, the most suitable testing conditions are investigated by changing L and t_1. The effects of bondline length l_{ad} and bondline thickness t_{ad} on ISSF were studied previously [9–13], the results in [9–13] are presented as follows. In [9–13], the specimen used by Park was analyzed. The total length of the specimen is 225 mm with adherend thickness t_1 = 7 mm and d = 10 mm, the adherend lengths are in the range 77.5 – 97.5 mm.

Fig. C.1(a) shows the effect of the bondline length l_{ad} under P/W = 14.15 N/mm [9–13]. It is seen that ISSF K_{σ,λ_1} decreases with increasing l_{ad}

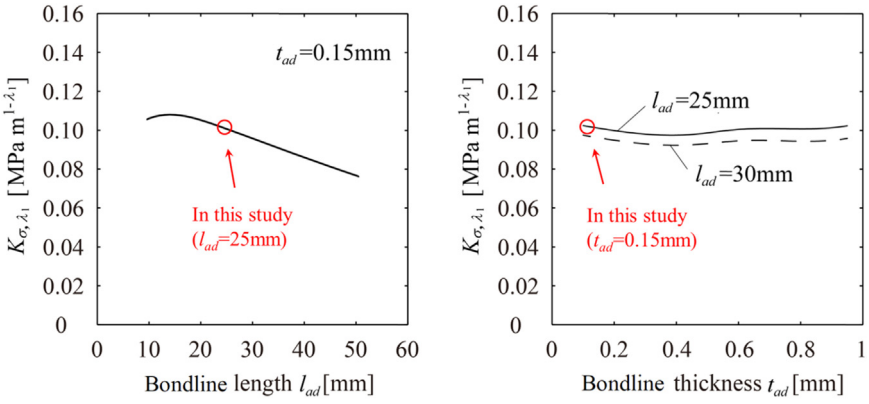

(a) (b)

Fig. C.1. (a) Relationship between ISSF K_{σ,λ_1} and bondline length l_{ad}; (b) Relationship between ISSF K_{σ,λ_1} and bondline thickness t_{ad} [9–13].

when $l_{ad} \geq 15$ mm. Fig. C.1(b) shows the effect of the bondline thickness t_{ad} [9–13]. The solid line and dashed line denote the values of K_{σ,λ_1} for $l_{ad} = 25$ mm and 30 mm, respectively. It is found that K_{σ,λ_1} is insensitive to t_{ad}.

References

[1] Nozu H, Kitada T. Recent progress of adhesive and sealant in the automobile industry. Trans Soc Auto Eng Jpn 1977;31(10):902–11. [in Japanese].
[2] J Soc Mater Sci. Adhesion and materials. Shokabo, Tokyo; 1996 [in Japanese].
[3] Lörinci G, Matuschek G, Fekete J, Gebefügi I, Kettrup A. Investigation of thermal degradation of some adhesives used in the automobile industry by thermal analysis/mass spectrometry and GC–MS. Thermochim Acta 1995;263:73–86.
[4] Barnes TA, Pashby IR. Joining techniques for aluminium spaceframes used in automobiles: part II — adhesive bonding and mechanical fasteners. J Mater Process Tech 2000;99(1-3):72–9.
[5] Xuemei W, Vijay G. Construction and characterization of chemically joined stainless steel/E-glass composite sections. Mech Mater 2005;37(12):1198–209.
[6] Jarry E, Shenoi RA. Performance of butt strap joints for marine applications. Int J Adhes Adhes 2006;26(3):162–76.
[7] Encinas N, Oakley BR, Belcher MA, Blohowiak KY, Dillingham RG, Abenojar J, Martínez MA. Surface modification of aircraft used composites for adhesive bonding. Int J Adhes Adhes 2014;50:157–63.
[8] Noda NA, Miyazaki T, Li R, Uchikoba T, Sano Y. Dedbonding strength evaluation in terms of the intensity of singular stress at the interface corner with and without fictitious crack. Int J Adhes Adhes 2015;61:46–64.
[9] Miyazaki T, Noda NA, Li R, Uchikoba T, Sano Y. Debonding criterion for single lap joints from the intensity of singular stress field. J Jpn Inst Electron Packag 2013;16(2):143–51. [in Japanese].
[10] Miyazaki T, Noda NA, Uchikoba T, Li R, Sano Y. Proposal of a convenient and accurate method for evaluation of debonding strength. Trans Soc Auto Eng Jpn 2014;45(5):895–901. [in Japanese].
[11] Miyazaki T, Noda NA, Sano Y. A precise and efficient analytical method to obtain two distinct intensities of singular stress fields for single lap joint. J Jpn Inst Electron Packag 2018;21(2):166–77. [in Japanese].
[12] Miyazaki T, Noda NA. Evaluation of debonding strength of single lap joint by the intensity of singular stress field. J Phys Conf Ser 2017;842:012078.
[13] Noda NA, Li R, Miyazaki T, Takaki R, Sano Y. Convenient adhesive strength evaluation method in terms of the intensity of singular stress field. Int J Comput Methods 2018;15(1):1850085-01–30.
[14] Mintzas A, Nowell D. Validation of an H_{cr}-based fracture initiation criterion for adhesively bonded joints. Eng Fract Mech 2012;80:13–27.
[15] Qian Z, Akisanya AR. An experimental investigation of failure initiation in bonded joints. Acta Mater 1998;46(14):4895–904.
[16] Hattori T, Iwasa M. Fracture mechanics with bonding or contacting interfaces: ii. A stress singularity parameters on a bonding or contact edge. J Soc Mater Sci 2000;49(1):123–9. [in Japanese].
[17] Shibutani T. Evaluation of crack initiation at interfacial edge on the basis of fracture mechanics concept and application to electronics devices (Tutorial series: foundations for reliability analysis). J Jpn Inst Electron Packag 2004;7(7):639–44. [in Japanese].
[18] JIS K6850:1999, Adhesives-Determination of tensile lap-shear strength of rigid-to-rigid bonded assemblies [in Japanese].
[19] Ikegami K, Fujii T, Kawagoe H, Kyogoku H, Motoie K, Nohno K, Sugibayashi T, Yoshida F. Benchmark tests on adhesive strengths in butt, single and double lap joints and double-cantilever beams. Int J Adhes Adhes 1996;16(4):219–26.
[20] Nakajima A, Saito M, Hino H, Nishi K, Suzuki Y, Kodaka A. Experimental study on fundamental strength characteristics of adhesive connection between steel members. J Adhes Soc Jpn 2011;47(2):53–9. [in Japanese].
[21] Park JH, Choi JH, Kweon JH. Evaluating the strengths of thick aluminum -to-aluminum joints with different adhesive lengths and thicknesses. Compos Struct 2010;92:2226–35.
[22] Yuuki R., Mechanics of interface. Baifuukann, Tokyo [in Japanese]; 1993.
[23] Bogy DB. Edge-bonded dissimilar orthogonal elastic wedges under normal and shear loading. Trans ASME J Appl Mech 1968;35:460–6.
[24] Bogy DB. Two edge-bonded elastic wedges of diffkkkerent materials and wedge angles under surface tractions. Trans ASME J Appl Mech 1971;38:377–86.
[25] Dundurs J. Discussion: “edge-bonded dissimilar orthogonal elastic wedges under normal and shear loading”. Trans ASME J Appl Mech 1969;36:650–2.
[26] Zhang Y, Noda NA, Wu PZ, Duan ML. A mesh-independent technique to evaluate stress singularities in adhesive joints. Int J Adhes Adhes 2015;57:105–17.
[27] Zhang Y, Noda NA, Wu PZ, Duan ML. Corrigendum to A mesh-independent technique to evaluate stress singularities in adhesive joints [Int J of Adhes Adhes, 2015; 57:105-117]. Int J Adhes Adhes 2015;60:130.
[28] Adams R, D, Peppiat N, A. Stress analysis of adhesive-bonded lap joints. J Strain Anal Eng 1974;9(3):185–96.
[29] Arai M, Kobayashi H. Adhesively bonded lap joints: fracture mechanisms and strength evaluation. Trans Jpn Soc Mech Eng A 1998;64(619):74–9.
[30] Campilho RDSG, Moura de MFSF, Domingues JJMS. Numerical prediction on the tensile residual strength of repaired CFRP under different geometric changes. Int J Adhes Adhes 2009;29:195–205.
[31] Noda NA, Ren F, Takaki R, Wang Z, Oda K, Miyazaki T, Sano Y. Intensity of singular stress field over the entire bond line thickness range useful for evaluating the adhesive strength for plate and cylinder butt joint. Int J Adhes Adhes 2018;85:234–50.